INDONESIAN JOURNAL ON GEOSCIENCE
Geological Agency
Ministry of Energy and Mineral Resources

Journal homepage: http://ijog.bgl.esdm.go.id
ISSN 2355-9314 (Print), e-ISSN 2355-9306 (Online)

Magma Chamber Model of Batur Caldera, Bali, Indonesia: Compositional Variation of Two Facies, Large-Volume Dacitic Ignimbrites

Igan S. Sutawidjaja[1], Mega F. Rosana[2], and K. Watanabe[3]

[1]Geological Agency of Indonesia,
[2]Padjadjaran University,
[3]Kyushu University-Japan

Corresponding author: iganss12@gmail.com
Manuscript received: June 22, 2015; revised: June 25, 2015;
approved: July 10, 2015; available online: August 25, 2015

Abstract - Batur is one of the finest known calderas on Earth, and is the source of at least two major ignimbrite eruptions with a combined volume of some 84 km^3 and 19 km^3. These ignimbrites have a similar compositions, raising the question of whether they are geneticaly related. The Batur Ignimbrite-1 (BI-1) is crystal poor, containing rhyodacitic (68 - 70wt % SiO_2), white to grey pumices and partly welded and unwelded. The overlying Batur Ignimbrite-2 (BI-2) is a homogeneous grey to black dacitic pumices (64 - 66 wt % SiO_2), unwelded and densely welded (40 - 60% vesicularity), crystal and lithic rich. Phase equilibria indicate that the Batur magma equilibrated at temperatures of 1100 - 1300^{o}C with melt water contents of 3 - 6 wt%. The post-eruptive Batur magma was cooler (<1100^{o}C) and it is melt more water rich (> 6 wt % H_2O). A pressure of 20 kbar is infered from mineral barometry for the Batur magma chamber. Magmatic chamber model is one in which crystals and melt separate from a convecting Batur magma by density differences, resulting in a stratified magma chamber with a homogeneous central zone, a crystal-rich accumulation zone near the walls or base, and a buoyant, melt-rich zone near the top. This is consistent with the estimated magma temperatures and densities: the pre-eruptive BI-1 magma was hoter (1300^{o}C) and more volatile rich (6 wt % H_2O) with density 2.25 g/cm^3 than the BI-2 magma (1200^{o}C; 4 wt % H_2O) in density was higher (2.50 g/cm^3). Batur melt characteristics and intensive parameters are consistent with a volatile oversaturation-driven eruption. However, the higher H_2O content, high viscosity and low crystal content of the BI-1 magma imply an external eruption trigger.

Keywords: Batur caldera, ignimbrite, rhyodacite, dacite, melting zone, magma chamber model

How to cite this article:

Sutawidjaja, I.S., Rosana, M. F., and Watanabe, K., 2015. Magma Chamber Model of Batur Caldera, Bali, Indonesia: Compositional Variation of Two Facies, Large-Volume Dacitic Ignimbrites. *Indonesian Journal on Geoscience*, 2 (2) p.111-124. DOI:10.17014/ijog.2.2.111-124

Introduction

Sequence of Ignimbrites

The Batur Volcanic Complex (BVC; Figure 1), which covers about 2,300 square kilometres in the southern and eastern part of Bali Island of Indonesia, has two large calderas that their formation are interpreted correlated with thick sequences of the exposed ignimbrites. Large explosive eruptions have been identified during Batur volcanic activities, producing rhyodacitic up to dacitic pyroclastic deposits. Two separate ignimbrite sheets have been recognized; the source areas for these are correlated to the caldera formations of Batur. Basalt to basaltic andesite lavas and pyroclastic deposits are interlayered with and underlie the ignimbrite sequences, particularly in the southem slope of the caldera. Other more mafic lavas that are distinguishable lithologically from the pre-caldera volcanics are recognized as pillow-basalts.

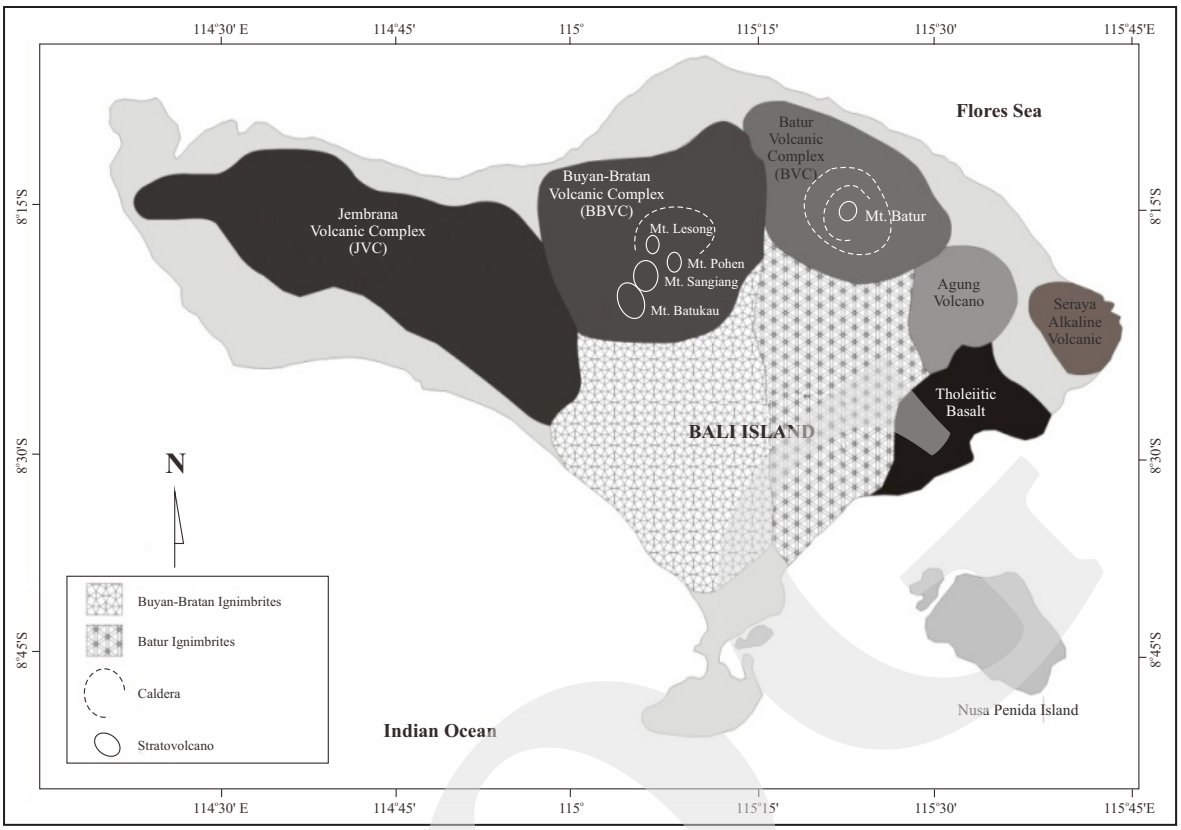

Figure 1. Bali volcanic complex and the distribution of ignimbrites.

Volcanologists that have examined Batur caldera and areas elsewhere, largely the ignimbrites, have questioned aspects of the locally established sequence. Marinelli and Tazieff (1968) believed that the paroxysm phase of the Batur caldera formation occurred 22,000 years BP, and produced rhyodacitic ignimbrite, followed by explosions of rhyodacitic pumice and bandaite blocks from the Caldera-II (C-II; Figure 2), culminated in the major ignimbrite eruption about 23,700 years B.P. and were followed by periodic strombolian eruptions of the basaltic magma that forms the core of this chamber.

Sutawidjaja (2009) found an indication that major revisions are required in the previously used stratigraphy. The evidence has come from ^{14}C dating of partially and densely welded ignimbrites. Charcoal found within the partially welded ignimbrite, BI-2 has given an age of 20,150 years B.P. Another charcoal found within the partially welded ignimbrite, BI-1 has an age of is 29,300 years B.P. Marinelli and Tazieff (1968) believed that the paroxysm phase of the Batur caldera formation occurred 22,000 years B.P., and produced rhyodacitic ignimbrite, followed by explosions of rhyodacitic pumice and bandaite blocks from the Caldera II. Follow up work by Wheller and Varne (1986) suggested that the explosive eruptions of highly fractionated dacitic liquids culminated in the major ignimbrite eruption about 23,700 years B.P. and were followed by periodic strombolian eruptions of the basaltic magma that forms the core of this chamber. Reubi and Nicholls (2004) found the significant differences in trace element contents between the parental melts, likely to reflect variable degrees of depletion of a MORB-like mantle wedge.

A volcanic activity associated with Batur caldera began in the Recent time with the eruption of the 0.3 Ma BI-1 rhyodacitic ignimbrite (Watanabe, 2010). This was followed by another caldera-forming event, which produced the dacitic BI-2. Post-eruption resurgence of the Batur magma led to the formation of an elongate block of intracaldera pumice cone known as the Caldera-I (C-I; Figure 2), and post-caldera volcanism produced

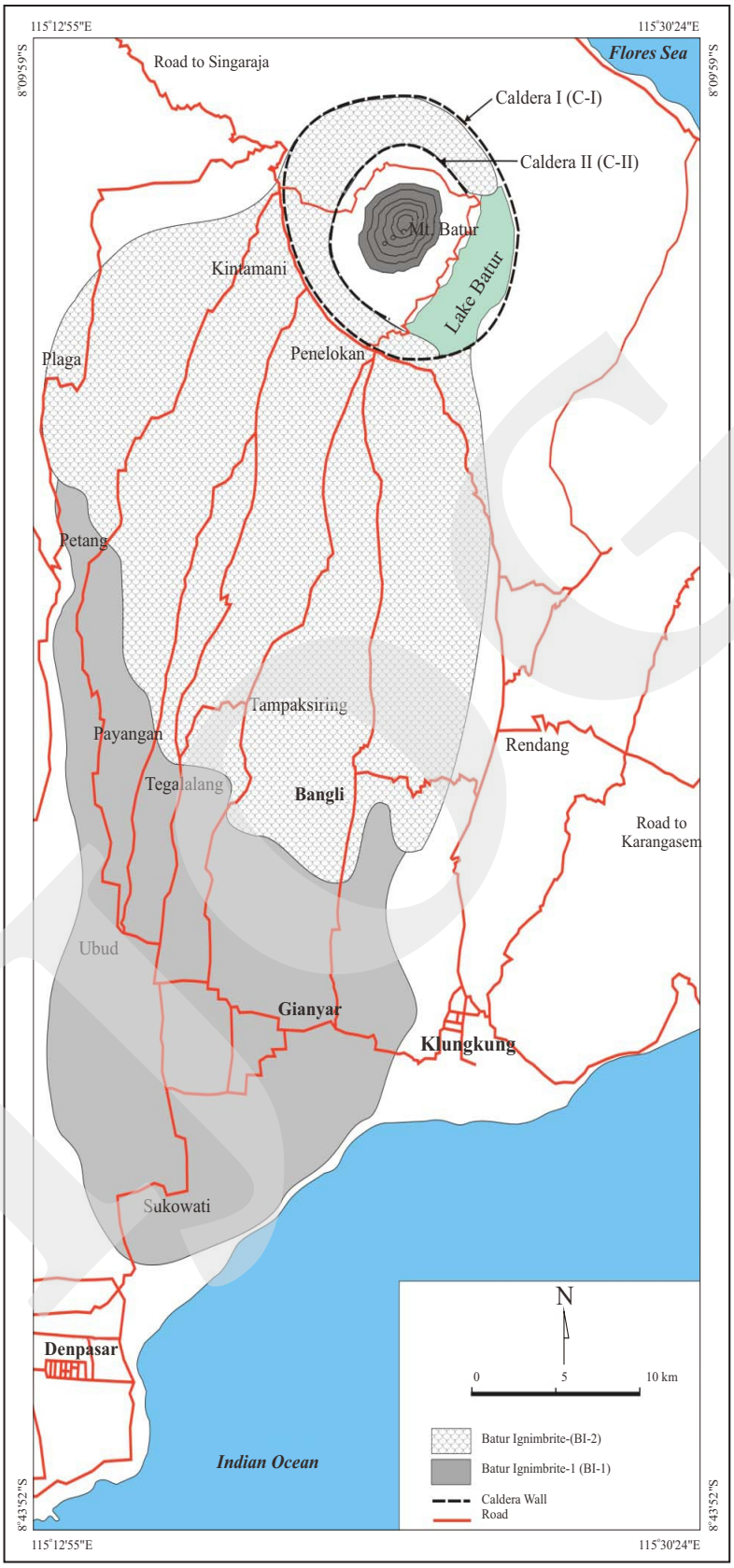

Figure 2. Map showing the distribution of BI-1 and BI-2 ignimbrites based on a line connecting their most distal known outcrops. The BI-1 is covered both within the C-I and in the outflow sheets by the BI-2, and only crops out in the valleys and in the C-II wall.

several small dacitic and andesitic domes along the center of the resurgent block and within the moat, such as dacitic Payang Pumice Cone and dacitic lava plug, and andesitic Bunbulan Cone and andesitic Bunbulan Dome. These post-caldera cones have not been dated.

BI-1 ignimbrite is a crystal-poor, homogeneous rhyodacitic ignimbrite with an estimated outflow volume of 84 km^3 (Sutawidjaja, 2009). Available ^{14}C date from the charcoal gave an age between 29,300 years B.P. (Sutawidjaja, 2009). The BI-1 ignimbrite comprises two main facies (Figure 3): a lower, partly-welded and non-indurated facies with abundant distinctive pumice clasts, and an upper facies, which has been indu-

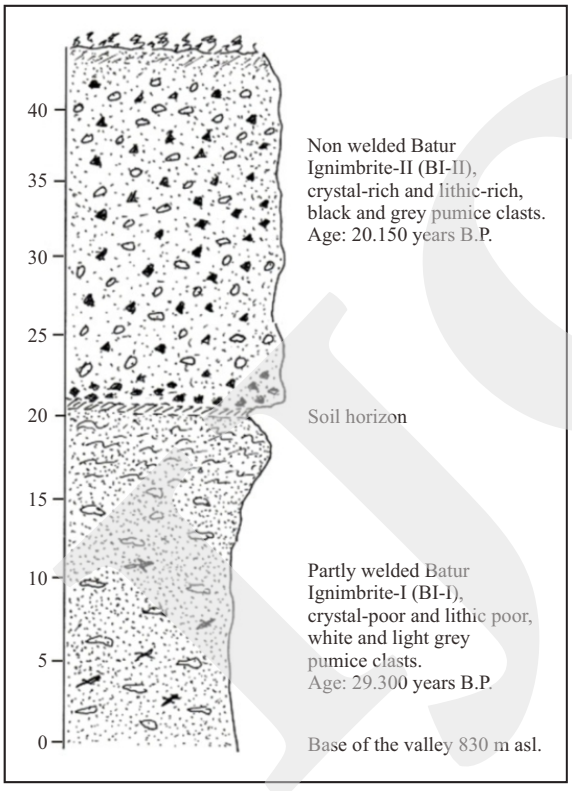

Figure 3. Stratigraphic section and ages of the Batur Ignimbrites.

rated by vapour-phase alteration. Locally, there is a thin (<50 cm) plinian air-fall deposit at the base, which contains small, aphyric pumice clasts.

On the uppert part of BI-1, the BI-2, is a crystal-rich, moderately lithic-rich dacitic ignimbrite comprising an intracaldera and outflow facies with a combined estimated volume of 19 km^3 (Sutawidjaja, 1990). ^{14}C age dating of charcoals from this unit has 20,770, The intracaldera facies of the resurgent block is characterized by densely welded and devitrified ignimbrites. The BI-2 outflow typically occurs as a single flow unit 30 - 10 m thick, which locally is underlain by a surge deposit and a soft ash and pumice-rich layer. The homogeneous, lithic-rich BI-2 is generally moderate to unwelded and shows various degrees of devitrification. It is rich in lithic fragments, and also relatively pumice poor.

Geological evidence for a hiatus between the eruption of the BI-1 and the overlying BI-2 is lacking. However, given the arid climate of the region and the inefficiency of erosion, a considerable hiatus could go unnoticed. The K-Ar age dating of the two ignimbrites is of insufficient precision to constrain the repose time between eruprions.

Methods and Analytical Techniques

Whole-rock major and trace elements of Ba, Cr, Rb, Sr, V, Y, Zn, Zr, and Nb were determined by X-ray fluorescence spectrometry (Philips PW 2400 and Siemens SRS 303 AS with Rh clasts) on fused glass discs and pressed powder briquettes. All isotopic analyses were carried out on unspiked whole-rock powders. Samples were dissolved by conventional digestion methods and Pb, Sr, and Nd were separated using standard anion (Pb) and cation (Sr, Nd) exchange techniques (exchange resins for Pb: Bio Rad AG1-X8, 100-200 mesh; Sr, Nd: Bio Rad AW 50 W-X8, 100-200 mesh; Nd: di (2-ethylhexyl)-orthophosphoric acid (HDEHP)-coated Teflon powder). Isotope ratios were determined on a Finnigan MAT 262 multicollector mass spectrometer (equipped with Faraday collectors) operating in a static mode.

Major element analyses of melt inclusions in quartz and matrix glass separates were determined by electron microprobe analysis (Cameca SXl00). Melt inclusions were generally devitrified, and had to be heated for rehomogenization in a pressurized gas vessel using Ar as a pressure rhedium. Crystals were placed in an Au capsule, pressurized and then heated by a graphite furnace. Run

conditions of heating were 800°C and 500 MPa for 24 hours. The quenching rate was ~10°C/s. After heating, melt inclusions generally appeared transparent, homogeneous without bubbles.

Trace element compositions of glass were determined by secondary ion mass spectrometry (SIMS) on a modified CAMECA 3F at the Center for Geological Survey, Geological Agency of Indonesia. A 1 nA ^{16}O primary beam with17 keV impact energy was focused on the sample surface to a spot diameter of ~20 µm. The secondary column was setup for low mass resolution with entrance and exit slits wide open, a 150 µm field aperture and a 40 eV bandpass. Energy filtering to avoid molecular interferences was performed by applying a -75 V offset to the sample. Secondary ions were detected by an electron multiplier system. For quantification, $^{30}Si+$ was analysed as a reference mass.

Results

Petrography and Mineral Chemistry

Three types of pumices are distinguished in the Batur Ignimbrite-2 (BI-2). The main type is crystal-rich pumice that contains 30 - 40% crystals comprising plagioclase, quartz, hornblende, minor sanidine, and pyroxene, and accessory magnetite, titanite, ilmenite, apatite ± allanite (Table 2). The pumices range in size from a few centimetres to >30 cm and are relatively dense, with 40 - 60% vesicularity (Table 2).

At several localities, the BI-2 ignimbrite also contains fine-grained, grey, lithic-rich and crystal-rich (40% crystals) pumice inclusions that occur as individual clasts in the ignimbrites or included in the crystal-rich pumices described above. The grey pumice inclusions have 40 - 50% vesicularity, and show no signs of textural disequilibrium with their host pumice clasts. They have a dominantly fine-grained matrix (<0.5 mm) of plagioclase, biotite, hornblende, clinopyroxene, minor orthopyroxene, and accessory magnetite, ilmenite, titanite and apatite (Table 2). Set within the fine-grained matrix are some large phenocrysts (> 1 mm), similar to those of the host pumice. The overall percentage of ferromagnesian minerals in the grey pumice inclusions is fairly constant, but the hbl:cpx ratio varies greatly (Table 1). Some samples display an ophimottled texture, and glomerocrysts of plagioclase and of hornblende + clinopyroxene are also present. Rare, crystal-poor (1 - 10% crystals) rhyodacitic pumices constitute the third type of pumice in the BI-2. These pumices typically occur in the non-indurated, crystal-poor basal zone of the ignimbrite and resemble the rounded, non-tubular crystal-poor pumices in the BI-1.

Mineral compositions determined by XRF are summarized in Table 1 and 2, and the main features of mineral petrography and composition are summarized briefly here. Plagioclase is the dominant feldspar and most abundant phenocryst in all BI-2 pumice and BI-1 pumice types. It is subhedral to anhedral, generally cracked, and exhibits a variety of zoning pattems. Plagioclase phenocrysts in BI-1 crystal-rich pumices and grey pumice inclusions have similar average core and rim compositions of An_{38-49} and An_{35-41}, respec-

Table 1. Modal Analyses of Batur Ignimbrite-I Pumices

	BL 02	BL03A	BL 03B	BL 05B	BL 05C	BL 06	BL 07A	BL 07B	BL 08	BL 09	BL 10	BL 11	BL 12	BL 13	BL 14	BL 15	BL 16
Pl	18.71	17.84	14.96	16.71	18.32	20.41	21.73	22.16	21.87	19.48	15.72	14.89	12.78	19.21	22.24	17.49	16.87
Q	19.42	18.56	18.24	17.85	17.89	18.69	18.51	20.02	19.21	19.27	19.76	19.84	18.04	19.62	20.06	18.67	17.35
or	21.36	20.45	19.47	18.76	21.82	22.32	21.73	18.93	20.87	21.72	22.24	22.37	18.85	21.43	22.51	20.37	18.97
ab	46.27	44.68	39.86	46.75	47.82	39.64	47.56	48.71	46.69	44.82	38.24	38.36	49.09	47.24	38.25	42.18	45.57
an	8.72	7.23	8.33	9.12	9.26	10.27	9.44	8.53	7.49	7.32	8.37	6.98	6.91	6.86	10.94	7.39	9.25
di	0.73	0.84	0,97	1.37	1.92	0.83	0.77	0.86	0.91	0.68	1.18	0.72	1.98	0.77	0.62	0.87	1.69
hy	2.73	2.92	2.87	3.21	3.19	2.67	2.89	2.76	3.05	3.14	2.79	2.46	3.24	3.21	3.04	1.79	2.63
ol	0	0	0	0	0	0	0	0	0	0	0	0	0		0		0
mt	2.67	2.91	2.63	2.74	2.93	3.02	3.06	2.79	2.81	2.67	2.98	2.96	2.58	2.97	3.09	2.84	3.05
il	1.08	1.02	1.11	1.13	1.07	1.01	1.12	1.06	1.09	1.03	1.09	1.11	0.99	0.12	1.11	0.11	1.13
ap	0.36	0.31	0.35	0.38	0.35	0.38	0.33	0.37	0.38	0.34	0.31	0.36	0.33	0.32	0.39	0.37	0.38
D.I.	82.57	82.69	83.02	81.79	82.92	81.58	83.51	83.69	82.83	80.76	81.96	82.76	83.98	81.88	80.83	82.76	81.89

Remarks: Pl = plagioclase; Q= quartz; or= orthoclase; ab= albite; an= anorthite; di= diopside; hy= hypersthene; ol= oligoclase; mt= magnetite; il= ilmenite; ap= apatite

Table 2. Modal Analyses of Batur Ignimbrite-II Pumices

	BL 01	BL 04	BL 05	BL 17	BL 18	BL 19	BL 20	BL 21	BL 22	BL 23	BL 24	BL 25	BL 26	BL 27	BL 28	BL 29
Pl	12.78	16.24	24.26	23.03	19.32	22.41	21.98	24.22	24.51	23.48	19.68	18.69	20.54	19.76	22.62	22.15
Q	14.82	14.21	13.87	14.46	13.79	13.73	14.78	13.91	13.93	14.21	13.73	12.43	15.32	15.42	15.47	14.78
or	16.35	15.93	16.37	14.48	14.76	15.49	16.72	15.23	16.15	16.56	15.89	14.8	16.73	16.87	17.59	16.72
ab	44.72	44.13	4369	43.76	43.72	43.75	43.87	43.8	44.67	45.78	44.72	43.34	44.07	44.21	44.33	43.87
an	12.49	13.73	14.12	13.87	14.01	14.03	13.13		12.49	11.01	13.65	14.07	12.63	11.57	11.41	13.13
di	1.68	1.79	2.43	2.51	2.13	1.89	1.83	2.74	2.68	2.52	2.87	2.91	2.05	1.87	1.74	1.83
hy	5.77	6.21	4.89	5.37	6.13	5.14	4.87	5.81	4.76	4.59	4.65	6.85	4.92	4.33	4.75	4.87
ol	0	0	0	0	0	0	0	0	0	0	0	0	0	0	0	0
mt	3.22	3.18	3.11	3.32	3.36	3.27	3.15	3.34	3.19	3.31	3.21	3.35	3.15	3.27	3.12	3.15
il	1.44	1.57	1.21	1.51	1.53	1.49	1.25	1.51	1.47	1.43	1.48	1.52	1.25	1.38	1.18	1.25
ap	0.53	0.61	0.46	0.57	0.62	0.58	0.41	0.67	0.61	0.62	0.69	0.74	0.43	0.43	0.41	0.41
D.I.	75.26	76.21	75.49	76.23	72.27	76.23	75.37	72.93	75.83	76.55	74.86	70.57	76.13	76.62	77.39	75.37

Remarks: Pl = plagioclase; Q= quartz; or= orthoclase; ab= albite; an= anorthite; di= diopside; hy= hypersthene; ol= oligoclase; mt= magnetite; il= ilmenite; ap= apatite

tively. The rims are similar to microphenocryst compositions in the BI-2 pumice samples (An_{35}).

Based on the classification of felsic rocks according to their molecular normative An-Ab-Or compositions after Baker (1979) diagram, and entirely up to the normative feldspar composition from BI-1 and BI-2, this diagram reflects an estimate of their original magma type (Figure 4), commonly with inclusions of plagioclase, magnetite, apatite, and zircon. Homogeneous, euhedral to subhedral amphibole crystals are subordinate to biotite in all pumice types. Compositionally, the amphiboles are mainly edenite and hornblende according to the nomenclature of Deer *et al.* (1992). Some compositions, particularly those from amphibole cores in grey pumice inclusions, are pargasitic. Magnetite and ilmenite are both present, and have no detectable exsolution or zoning. Zircon and colourless apatite are common accessories in both the BI-2 and BI-1 pumices, and yellow titanite is also present in BI-2 crystal-rich pumices and grey pumice inclusions.

Whole-Rock Geochemistry

The following characterization of the BI-1 and BI-2 compositions is based on unaltered pumice samples, with all analyses normalized to a 100% volatile-free basis. Only representative analyses are presented in Table 3 and Table 4. BI-1 data represent pumices from the lower, unwelded and non-vapour-phase altered facies of the ignimbrite, and all BI-2 pumice samples represent the outflow facies because the intracaldera BI-2 ignimbrite is welded, devitrified and altered. Chemical evidence for alteration is lacking and the compositions reported are considered to represent the erupted magmas.

All BI-2 and BI-1 pumices belong to the high-K suite of calc-alkaline magmas (Figure 5), and are metaluminous to weakly peraluminous with molar (Na+K)/Al between 0.6 and 0.9. and molar Al/(Ca+ Na+K) between 1.0 and 1.3. BI-2 crystal-rich pumices are dacitic to rhyodacitic, with 62 - 65 wt.% SiO_2 (Table 3), whereas the BI-1 pumices and BI-2 crystal-poor pumices are high-silica rhyodacitic, with 65 - 70 wt. % SiO_2 (Table 4). Two samples of BI-1 plinian pumice have 69 wt.% SiO_2. Grey pumice inclusions from the BI-2 ignimbrite range in composition from 61 to 65 wt. % SiO_2. Clasts of scoria and banded pumice exist in the BI-1 but are very rare and only one sample of each could be collected; thus their significance cannot be interpreted. The black pumice clast has a dacitic composition (64 wt. % SiO_2) and the banded pumice clast has a rhyodacitic composition (68 wt.%, SiO_2).

Major element oxide data of the BI-2 and BI-1 pumice samples form distinct groups on silica variation diagrams (Figure 6) separated by compositional gaps, and these groups correspond to the BI-2 clystal-rich pumices, the grey pumice inclusions in BI-2, and the BI-1 pumices. The BI-1 data show little or no systematic variation with silica because the samples are already at the high-silica end of magma differenriation. The other groups define regular and generally negative correlations of element oxides with silica excepting K_2O, which increases, and Na_2O, which shows no correlation (Figure 6). Both Na_2O and K_2O concentrations in the pumices are strongly

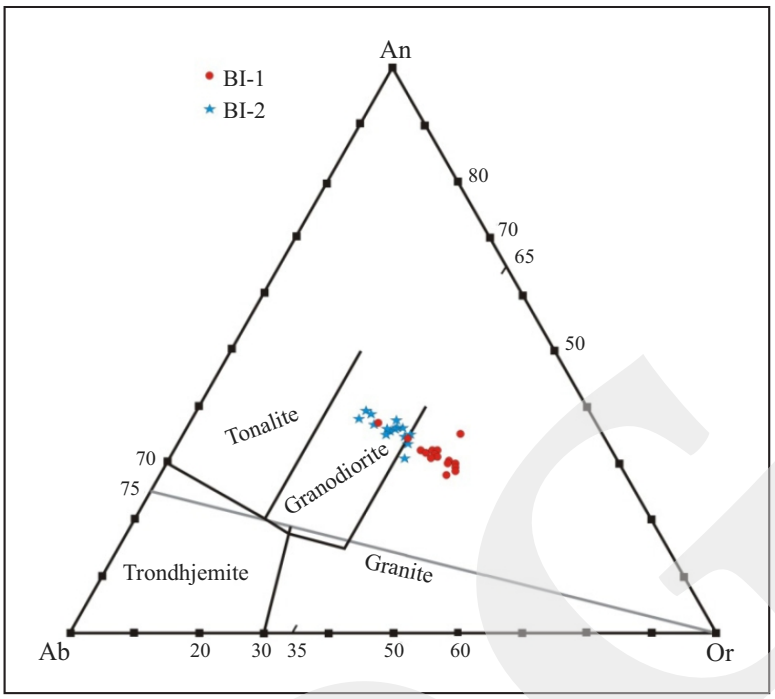

Figure 4. Ab-An-Or ternary plot of ignimbrite compositions from BI-1 and BI-2 based on the Baker (1979) diagram. The original fields of O'Connor (1965) are shown in a grey line.

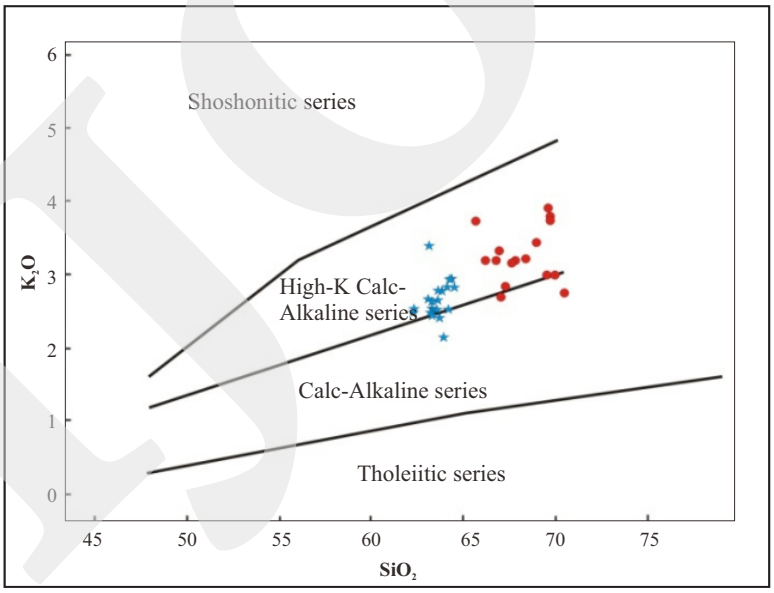

Figure 5. Almost all the BI-1 and BI-2 pumices belong to the high-K calc-alkaline magmas. Field from Peccerillo and Taylor (1976).

variable at higher SiO_2 contents, whereas the total alkali ($Na_2O + K_2O$) remains relatively constant.

The BI-2 grey pumice inclusions as a group have the lowest silica contents and the BI-1 pumices the highest. The BI-2 crystal-rich pumice group plots between these two extremes. In terms of all diagrams plotted in Figure 6, the three main groups of samples are collinear. The abundant basaltic lithic types tend to plot outside the main groups of samples and in some cases they bridge the compositional gaps between them. Thus the rare crystal-rich BI-2 pumices

Table 3. Representative Chemical Compositions of Batur Ignimbrite-I Pumices

	BL 02	BL 03 A	BL 03 B	BL 05 B	BL 05 C	BL 06	BL 07 A	BL 07 B	BL 08	BL 09	BL 10	BL 11	BL 12	BL 13	BL 14	BL 15	BL 16
SiO_2	69.55	68.99	67.08	69.96	69.83	69.68	70.48	69.57	68.44	67.01	67.31	69.82	67.77	67.78	65.68	66.19	66.77
TiO_2	0.52	0.53	0.59	0.46	0.46	0.46	0.47	0.48	0.54	0.59	0.51	0.49	0.52	0.52	0.57	0.62	0.59
Al_2O_3	15.09	15.23	16.42	14.64	14.53	14.52	14.46	14.57	15.33	5.45	14.98	14.65	15.04	15.07	15.12	15.81	15.62
FeO*	3.91	4.19	5.51	4.38	4.53	4.51	4.39	4.57	4.62	5.46	6.74	4.19	2.76	4.81	4.06	5.04	4.16
Fe_2O_3	2.68	2.79	2.63	3.21	3.03	2.46	2.87	2.96	2.68	2.59	2.93	2.87	2.76	2.84	3.04	3.22	3.22
MnO	0.12	0.12	0.16	0.13	0.15	0.14	0.11	0.14	0.14	0.16	0.16	0.11	0.18	0.17	0.14	0.09	0.17
MgO	2.07	2.51	2.76	1.64	1.94	1.92	1.69	1.99	2.54	1.94	1.94	2.18	0.46	0.43	0.76	0.59	0.65
CaO	0.44	0.55	0.52	0.44	0.53	0.49	0.41	0.52	0.55	0.24	0.32	0.57	2.03	2.01	2.5	2.58	2.47
Na_2O	5.13	4.33	4.12	5.19	4.19	4.33	5.09	4.11	4.47	5.63	5.04	4.11	5.53	5.48	4.39	5.06	5.35
K_2O	2.98	3.41	2.68	2.99	3.77	3.79	2.75	3.89	3.21	3.31	2.81	3.72	3.17	3.19	3.7	3.18	3.19
P_2O_5	0.19	0.17	0.17	0.16	0.07	0.15	0.15	0.15	0.17	0.22	0.21	0.14	0.14	0.13	0.16	0.17	0.16
Total	100	100	100	100	100	100	100	100	100	100	100	100	100	100	100	100	100
Sc	14	12	12	12	12	13	12	14	14	12	12	13	12	14	14	14	14
V	32	38	30	35	34	33	34	36	38	38	36	32	29	39	32	38	19
Cr	3	2	2	2	1	1	3	3	1	1	2	3	1	0	3	1	0
Ba	521	516	498	487	517	521	519	508	516	486	493	482	516	519	506	488	497
La	18	21	20	17	17	20	21	19	18	18	20	21	20	17	22	20	20
Ce	50	52	52	48	44	46	51	50	49	45	49	51	49	46	52	49	51
Ni	4	6	6	3	3	5	4	7	5	4	6	6	3	4	7	6	4
Cu	29	26	30	29	19	23	26	30	27	25	21	28	13	13	25	31	13
Zn	96	93	98	89	95	98	88	86	89	93	97	92	97	87	95	101	97
Zr	224	220	216	223	216	196	198	221	223	224	218	222	198	199	225	221	217
Nb	14	14	11	13	12	12	11	10	14	13	10	14	10	12	14	13	13
Ga	19	17	17	18	20	18	19	20	18	18	17	20	20	19	17	19	20
Pb	12	12	14	17	15	14	12	17	13	11	15	16	5	11	10	17	12
Rb	67	65	67	68	64	66	67	67	66	64	68	71	67	64	75	67	69
Sr	192	186	191	183	178	201	198	178	184	169	165	198	205	164	176	208	205
Th	6	6	8	4	5	7	7	4	5	4	8	8	3	6	8	7	7
U	2	2	2	2	1	2	1	1	1	2	2	2	1	2	2	2	2
Y	45	42	42	44	40	41	44	45	41	42	45	44	44	45	45	39	44

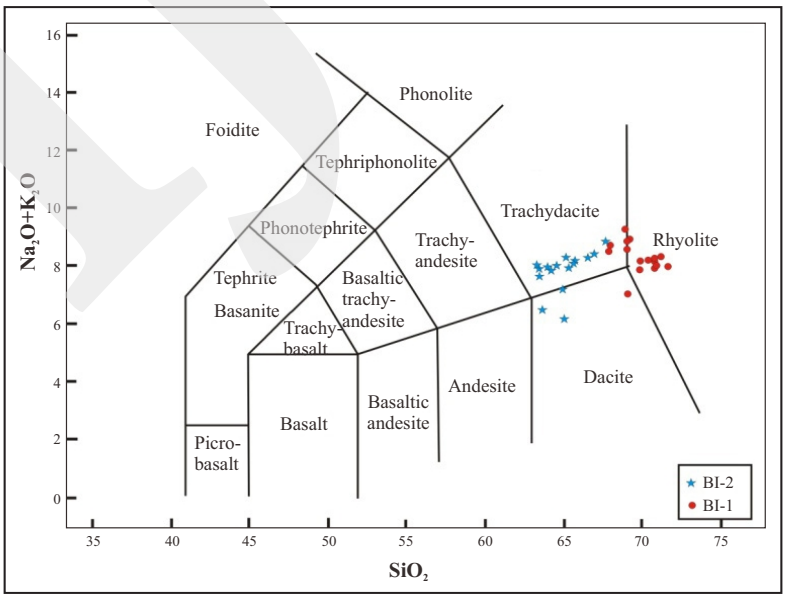

Figure 6. SiO_2 *vs* Na_2O+K_2O classification diagram for BI-1 and BI-2 showing the compositions of dacite to rhyolite. Field from Le Maitre (1989).

Table 4. Representative Chemical Compositions of Batur Ignimbrite-II Pumices

	BL 01	BL 04	BL 05	BL 17	BL 18	BL 19	BL 20	BL 21	BL 22	BL 23	BL 24	BL 25	BL 26	BL 27	BL 28	BL 29
SiO_2	62.38	63.74	64.03	63.1	63.25	63.11	64.23	63.49	63.62	63.91	64.29	62.29	64.47	63.58	64.35	63.31
TiO_2	0.8	0.73	0.64	0.49	0.8	0.78	0.65	0.79	0.78	0.74	0.76	0.79	0.65	0.65	0.61	0.85
Al_2O_3	14.62	16.93	16.61	14.12	16.22	16.02	16.23	15.96	15.78	15.73	15.95	16.13	16.08	16.02	15.72	15.71
FeO	2.63	2.33	2.24	2.21	2.37	2.41	2.81	2.63	2.69	2.65	2.51	2.47	2.56	2.47	2.31	2.39
Fe_2O_3	8.5	7.39	6.71	4.56	6.43	6.48	2.22	5.36	6.3	4.92	5.77	2.75	4.57	5.05	3.2	6.57
MnO	0.16	0.14	0.17	0.16	0.19	0.2	0.16	0.2	0.2	0.19	0.19	0.19	0.19	0.06	0.19	0.21
MgO	1.19	2.21	2.05	0.49	1.17	1.21	1.54	1.24	1.12	1.1	1.18	1.38	0.87	0.44	0.85	1.28
CaO	2.15	2.18	1.02	1.98	3.64	3.59	3.28	3.63	3.46	3.13	3.23	3.91	3.11	2.91	2.89	3.57
Na_2O	3.35	4.04	4.86	4.85	5.13	5.31	5.13	5.14	5.24	5.33	5.43	5.07	5.15	5.06	5.14	5.34
K_2O	2.53	2.42	2.14	3.37	2.48	2.64	2.85	2.56	2.62	2.76	2.49	2.48	2.82	2.76	2.92	2.51
P_2O_5	0.18	0.28	0.29	0.12	0.25	0.26	0.17	0.28	0.27	0.26	0.27	0.31	0.18	0.18	0.17	0.36
LOI	10.04	8.18	1.39	6.63	0.63	0.75	1.07	0.47	0.01	0.07	0.5	0.87	0.93	2.88	1.38	0.08
Total	100	100	100	99.86	100.2	100.3	99.7	100	99.4	98.86	100	99.57	99.96	99.59	99.42	99.78
Sc	14	21	19	15	10	12	15	17	16	13	23	16	15	15	14	17
V	57	49	54	54	38	47	41	30	23	24	20	66	31	41	30	36
Cr	2	1	2	3	1	1	2	1	1	1	7	2	3	3	2	1
Ba	473	456	479	466	493	506	469	447	445	432	457	414	486	476	473	455
La	19	17	15	19	18	19	19	15	15	15	10	15	18	19	17	18
Ce	42	45	41	47	48	47	47	45	46	40	43	44	48	47	48	48
Ni	6	4	7	5	4	8	5	4	4	4	9	9	5	4	3	4
Cu	22	27	29	22	13	15	22	18	14	29	25	20	21	19	15	17
Zn	93	89	94	97	103	98	92	91	86	99	89	99	78	81	94	107
Zr	163	178	183	188	191	198	193	160	164	154	189	144	191	191	192	158
Nb	9	11	11	11	11	11	12	9	8	9	4	9	11	12	12	10
Ga	18	17	17	17	17	19	18	19	19	18	19	19	19	19	19	17
Pb	9	11	7	10	11	11	11	8	7	9	8	9	9	8	10	9
Rb	63	59	61	65	61	63	59	50	54	51	50	44	63	60	64	48
Sr	225	248	271	148	153	244	253	288	279	273	282	273	264	256	234	279
Th	6	4	4	7	7	7	7	5	6	5	6	4	7	6	7	5
U	2	2	1	1	2	2	2	1	2	2	2	1	1	2	1	1
Y	41	39	40	42	41	43	41	41	42	37	37	38	40	35	39	42

are dacitic and plot in the field of BI-1 pumice whereas the brown-white banded BI-1 pumice has a composition intermediate between the BI-2 crystal-rich pumice and BI-1 pumice. The BI-1 scoria sample has SiO_2 contents corresponding to the lot-silica end of the BI-2 pumice range but it deviates from the latter in terms of MgO, Fe_2O and MnO (latter two diagrams not shown in Figure 6).

Trace element concentrations of BI-2 and BI-1 pumices also cluster in variation diagrams (Figure 7) but, unlike the major elements, the trace element variations within and among the different groups do not define collinear trends. The rhyodacitic samples, including BI-1 pumice and BI-2 crystal-poor pumice, are generally depleted in Zr and Sr, and enriched in Rb and Y relative to the dacitic BI-2 crystal-rich pumice and grey pumice inclusions. They show a much greater range in Ba and Rb/Sr values than the dacitic pumices.

The BI-2 crystal-rich pumices plot in or near the field of BI-1 pumices and share the same compositional trends in Figure 8. Interestingly, some of the considerable variation in element abundances for the BI-1 pumices correlates with geographical distribution of the out-flow ignimbrite. Pumices from the south and southwest of the caldera tend to have higher K_2O, Rb, and Y, lower Ba and Na_2O, than those from the west of the caldera. It should be noted that the composi-

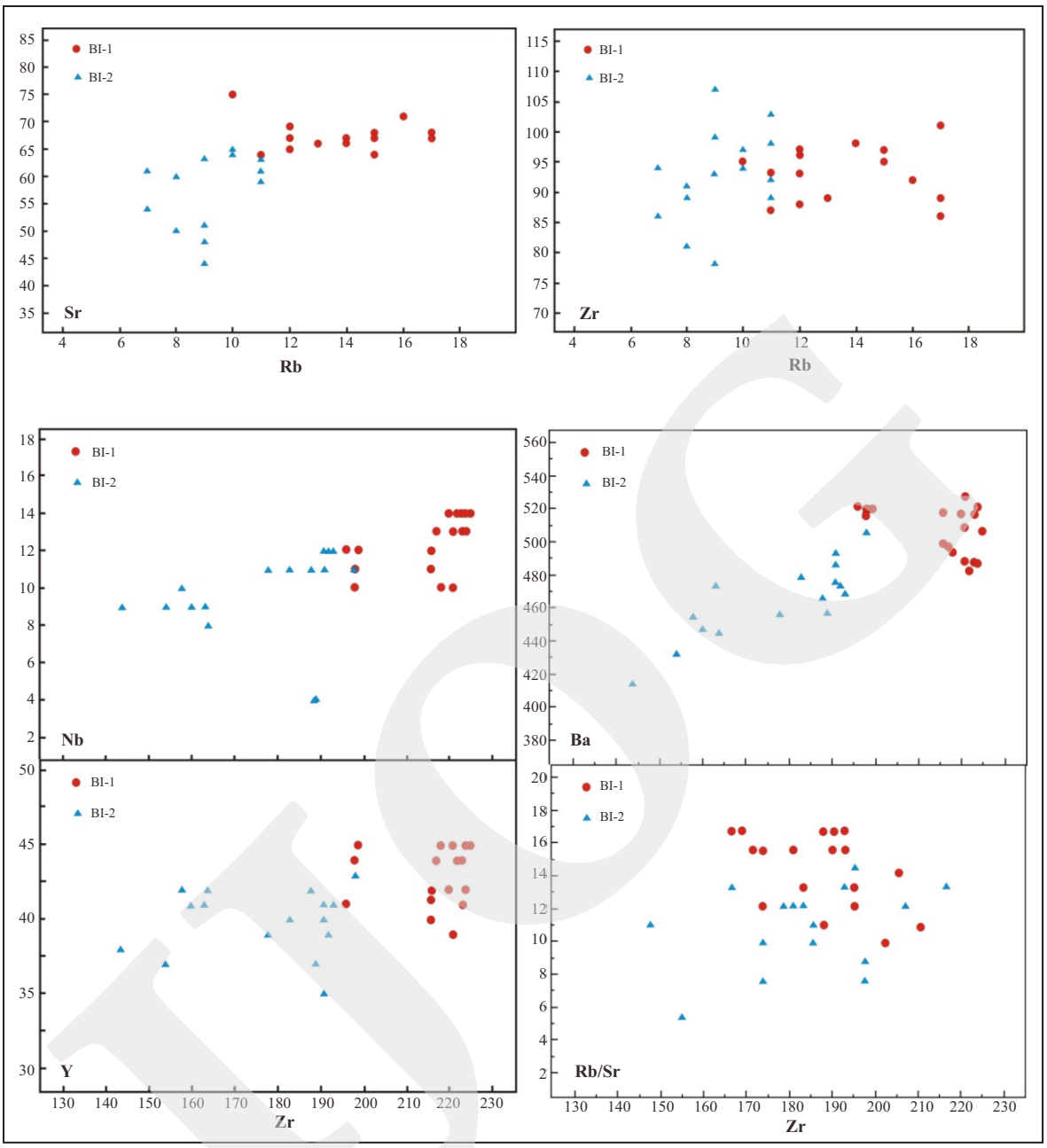

Figure 7. Trace element variation diagrams of BI-1 and BI-2 pumices.

tional range in BI-2 crystal-rich pumices is even greater than that of the BI-1 pumices but the variation in the BI-2 samples does not correlate with location.

Glass Composition

Glass compositions from quartz-hosted melt inclusions in two BI-2 crystal-rich pumice samples and from matrix glass separates of one BI-1 and two BI-2 pumices are presented in Table 4 and Figure 8. The BI-2 pumice glasses, both from melt inclusions and matrix separates, plot well within the compositional field of the BI-1 bulk pumice samples and resemble the crystal-poor BI-2 pumices. This implies that the compositional differences between the BI-2 crystal-rich pumice and BI-1 pumices are primarily a function of different crystal contents. The fractionation vectors show that the separate compositional groups defined by BI-2 crystal-rich pumice and BI-1

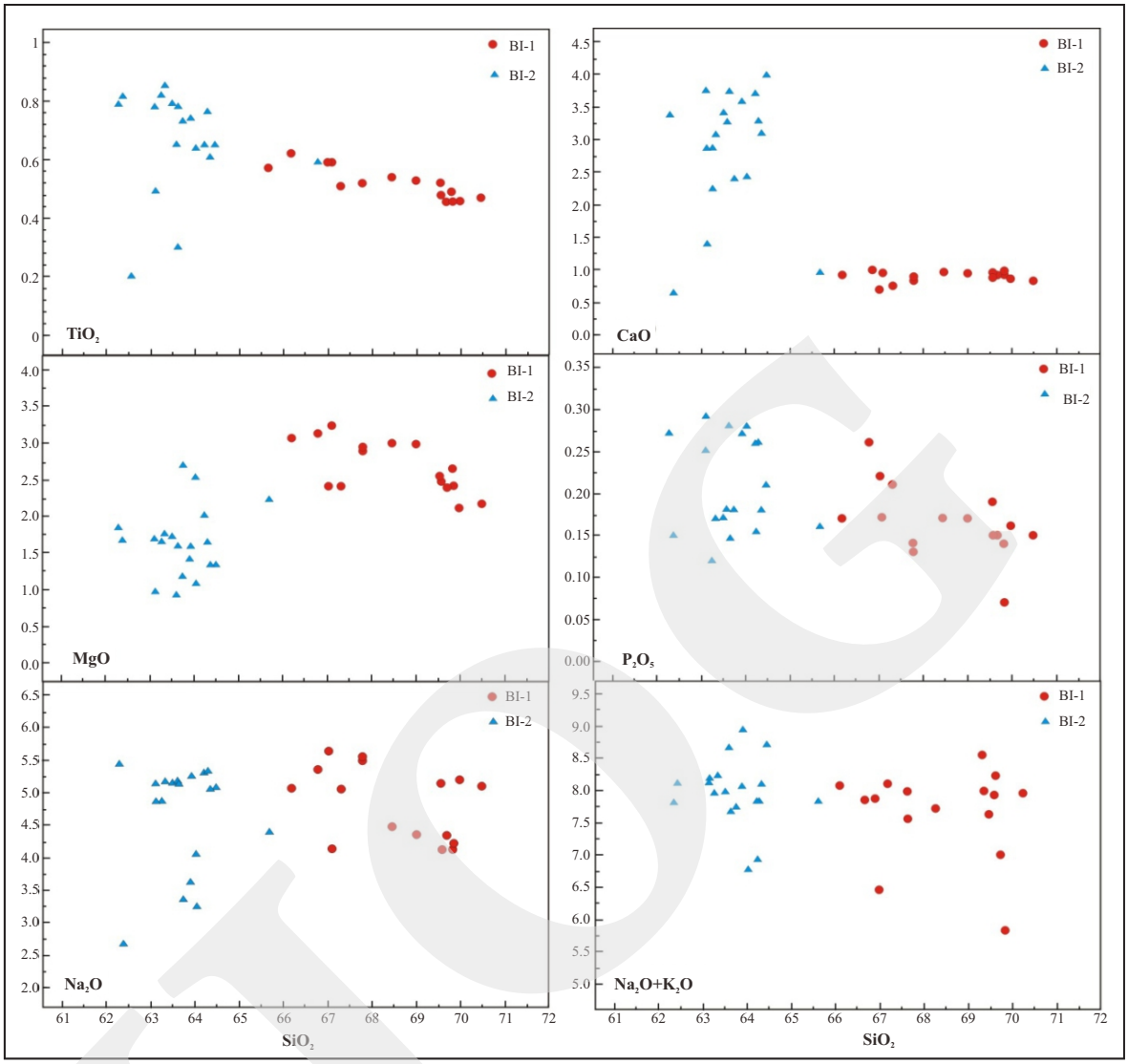

Figure 8. Major element variation diagrams of BI-1 and BI-2 pumices.

pumice can be related by simple fractionation of observed phases in the BI-2 samples. Also evident from Figure 8 is that the BI-1 glass is similar to the bulk pumice, as expected from the low crystal contents in the pumice, but the glass is slightly more fractionated (*i.e.* lower Sr and Ba contents) and has more variable Rb concentrations.

Discussion

The geochemical and petrological evidence shows that the BI-1 and BI-2 magmas are cogenetic, and can be related to each other by crystal fractionation. A physical model of crystal-liquid fractionation in the Batur magma chamber must be able to explain the extremely crystal-poor nature of the BI-1 ignimbrite and its considerable volume: the BI-1 and BI-2 outflow ignimbrites are more or less the same size (Sutawidjaja, 2009). It must also explain the homogeneity of the BI-2 ignimbrite and the presence of grey, crystal-rich pumice inclusions. The simplest model that accounts for all these features is one in which crystals and melt separate from a convecting Batur magma by density dififerences, resulting in a strarified magma chamber with a homogeneous central zone, a crystal-rich accumulation zone near the walls or base, and a buoyant, melt-rich zone near the top. This is

consistent with the estimated magma temperatures and densities: the pre-eruptive BI-1 magma was hoter (1300°C) and more volatile rich (6 wt. % H_2O) than the BI-2 magma (1100°C; 4 wt. % H_2O), and in density was higher 2.50 g/cm^3 than BI-1 (2.25 g/cm^3). The average pressure yield 10 kb at 1100 and 1300°C, respectively, which corresponds to 7 - 9 km depth (Figure 9). Evidence for convection in the BI-1 magma is provided by the remarkable mineralogical and chemical homogeneity of the BI-2 crystal-rich pumices, which show no refilling basalt magma and no mixing with basalt in the flow unit or distance from source.

It has been suggested that magma chamber shape plays an important role in determining the effectiveness of side-wall convective fractionation vs differentiation by crystal settling in magma chambers (de Silva and Wolff, 1995). Large-volume, homogeneous igrimbrites such as the BI-1 ignimbrite are thought to erupt from magma chambers with high aspect ratios (*i.e.* sill-shaped), in which side-wall crysrallization is considered is produced cumulate of crystal mashes because crystallization proceeds mainly in the main part of the convecting magma.

A schematic model for the Batur magma chamber that takes into consideration these arguments is presented in Figure 9. Fractionation of the convecting rhyodacitic and dacitic magma in a sill-like chamber led to the generation of a zone of buoyant melt at the top of the chamber. According to Marsh (1981), constraints from crystal packing make melt extraction possible until crystallization exceeds 50 - 60%. This evolved residual melt was effectively separated from the convecting dacitic magma by density differences. Continued differentiation in the zone by side-wall fractionation may have produced the zonation of cumulate crystal mash observed in the BI-1 magma.

The BI-1 magma did not mix with the BI-2 magma during eruption, implying that it was too thick, or the discharge rate too low, for the critical draw-down depth to reach the BI-2 magma below. The relationship between discharge rate and draw-down depth can be estimated by the method of Blake and Ivey (1986). Eruption rates of the BI-1 ignimbrite are unknown but assuming

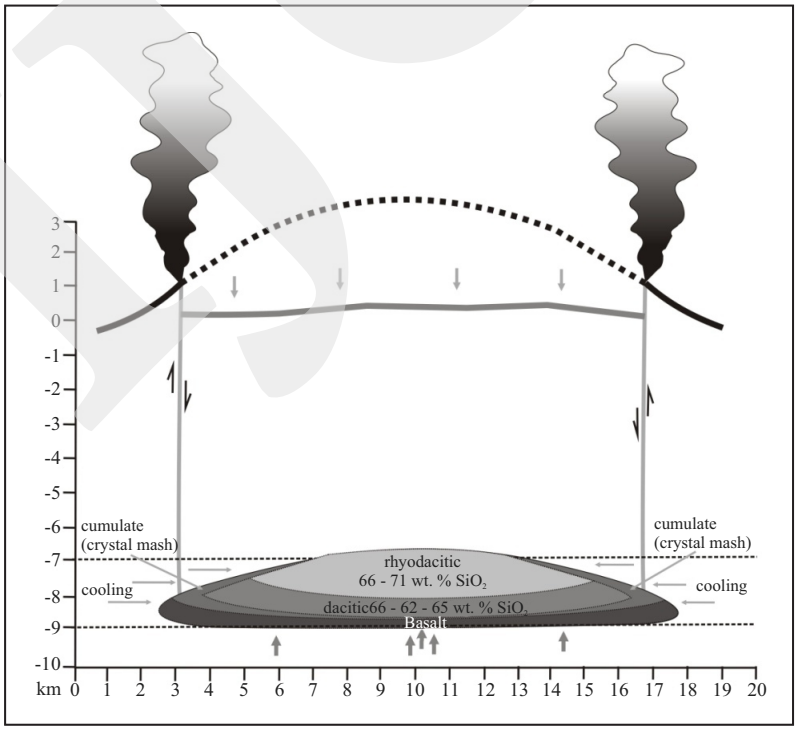

Figure 9. Zoned magma chamber of BI-1 and BI-2 based on inferred pre-eruptive condition without no refilling basalt magma and no mixing with basalt. Grey arrow lines indicate movement of liquid magmas after their defferentiated melts.

rates typical of ignimbrite eruptions (104 - 105 m^3/s), a thickness of at least 100 - 200 m for the BI-1 magma is required to prevent draw-down reaching the BI-2 magma beneath.

Conclusions

The results of this geochemical and field study of the ignimbrites associated with the BVC lead to the following conclusions:

- the crystal-rich dacitic BI-2 (19 km^3) and the crystal-poor rhyodacitic BI-1 (84 km^3) represent cogenetic magmas. These ignimbrites have a similar compositions, the BI-1 is crystal poor, contains rhyodacitic (68 - 70 wt. % SiO_2) white to grey pumices and partly welded and non welded. The overlying Batur Ignimbrite-II (BI-2) is a homogeneous grey to black pumice is dacitic (64 - 66 wt. % SiO_2), non welded and densely welded, crystal and lithic rich.
- The composition of BI-2 pumice and BI-1 rhyodacitic pumice clasts reveals a large compositional range for many trace elements in the chemically evolved cap of the zoned pre-eruptive magma chamber. The BI-2 data indicate that the greatest variation and the most evolved compositions are present in outflow ignimbrite, from the north to the south of the caldera. This is interpreted as reflecting zoning in the magma, whereby the distal outflow may represent the latest deposition of the eruption.
- The similarity in geochemical and field characteristics between the BI-2 volume, crystal-rich ignimbrite in the BVC implies a common petrogenesis, and other large volume of BI-1, crystal-poor ignimbrite indicates the current models that invoke crustal melting as the predominant magma-generation process. Phase equilibria indicate that the Batur magma equilibrated at temperatures of 1100 - 1300°C with melt water contents of 3 - 6 wt. %. The post-eruptive Batur magma was cooler (<1100°C) and its melt more water rich (> 6 wt. % H_2O). Thermal constraints, together with a lack of chemical or petrographic evidence for interaction with upper crust at the level of the Batur magma chamber, rule out large-scale crustal melting at this depth (7 - 9 km).
- Identification of the crustal material involved in the Batur magma source and the proportion of crustal to mantle-derived material is extremely difficult because of the heterogeneity of pre-Batur basement. These basement rocks completely different with Java and Lombok rocks, and based on the tectonomagmatic geochemical discriminant, Bali rocks felt in the area of spreading center island. This is assuming that Bali island was built by a submarine basaltic, and indicated by precentages of olivine in BVC.

Acknowledgment

This study was carried out as part of the desertation. Thanks are due to numerous lecturers and colleagues in Padjadjaran University for their support, including many productive discussions. We would like to thank the staffs at the Geological Agency in Bandung, Indonesia, for logistical and financial support in the field, and Prof. Adjat Sudradjat and Prof. Tetsuo Kobayashi in Kagoshima for constructive discussions mainly in the field. Major and trace elements analyses were carried out at the Center for Geological Survey, who gratefully acknowledges assistance support. The authors acknowledge the crucial contributions to all our colleagues which has greatly improved the presentation of the results.

References

Baker, F., 1979. Trondhjemite: Definition, environment and hypotheses of origin. *In*:Baker, F. (ed.), T*rondhjemites, dacites and related rocks*. Elsevier, Amsterdam, p.1-12. DOI:10.1016/B978-0-444-41765-7.50006-X

Blake, S. and Ivey, G. N.,1986. Magma-mixing and withdrawal dynamics of stratified reser-

voirs. J*ournal of Volcanology and Geothermal Research* 27, p.153-178. DOI:10.1016/0377-0273(86)90084-3

Deer, W. A., Howic, R. A., and Zussman, J.,1992. *An Introduction to the Rock-forming Minerals*, 2nd edition. Harlow, UK: Longman.

de Silva, S. L. and Wolff, J. A.,1995. Categorized magma chamber; magma chamber geometry influence on the sidewall convective fractionation. *Journal of Volcanology and Geothermal Research* 65, p.111-118.

Le Maitre, R. W. (ed.), 1989. *A frozen classification Rocks and Glossary*. Oxford: Blackwell.

Marinelli, G. and Tazieff, H., 1968. L'ignimbrite et la caldera de Batur (Bali, Indonesie). *Bulletin Volcanologique,* 32, p.89-120. DOI:10.1007/BF02596587

Marsh, B. D., 1981. On the crystallinity, probability of occurrence, and rheology of lava and magma. *Contributions to Mineralogy and Petrology,* 78, p.85-98. DOI:10.1007/BF00371146

O'Connor, J. T., 1965. A classification of quatrz rich igneous rock based on feldspar ratios. *US. Geological Survey Professional Paper*, B525, p.79-84.

Peccerillo, R. and Taylor, S.R., 1976. Geochemistry of Eocene calc-alkaline volcanic rocks from the Kastamonu area, northern Turkey. *Contribution to Mineralogy and Petrology*, 58, p.63-81. DOI:10.1007/BF00384745

Reubi, O. and Nicholls, I.A., 2004. Magmatic evolution at Batur volcanic field, Bali, Indonesia: petrological evidence for polybaric fractional crystallization and implications for caldera-forming eruptions. *Journal of Volcanology and Geothermal Research,* 138, p.345-369. DOI:10.1016/j.jvolgeores.2004.07.009

Sutawidjaja, I.S., 1990. *Evolution of Batur caldera, Bali, Indonesia*. A thesis of MSc, Victoria University of Wellington, New Zealand, unpublished.

Sutawidjaja, I.S., 2009. Ignimbrite analyses of Batur caldera, Bali, based on ^{14}C dating. *Indonesian Journal of Geology,* 4 (3), p.189-202. DOI:10.17014/ijog.vol4no3.20094

Watanabe, K., Yamanaka, T., Harijoko, A., Saitra, C., and Warmada, I.W., 2010. Caldera activities in North Bali, Indonesia. *Journal of SE Asian Applied Geology*, 2 (3), p.283-290.

Wheller, G.E. and Varne, R., 1986. Genesis of dacitic magmatism of Batur volcano, Bali, Indonesia: Implications for the origin of stratovolcano calderas. *Journal of Volcanology and Geothermal Research,* 28, p.363-378. DOI:10.1016/0377-0273(86)90031-4